Synergistic Effect of Hierarchical Nanostructured MoO$_2$/Co(OH)$_2$ with Largely Enhanced Pseudocapacitor Cyclability

Kalele Mulonda Hercule,[†] Qiulong Wei,[†] Aamir Minhas Khan, Yunlong Zhao, Xiaocong Tian, and Liqiang Mai*

State Key Laboratory of Advanced Technology for Materials Synthesis and Processing, WUT-Harvard Joint Nano Key Laboratory, Wuhan University of Technology, Wuhan 430070, China

Ⓢ Supporting Information
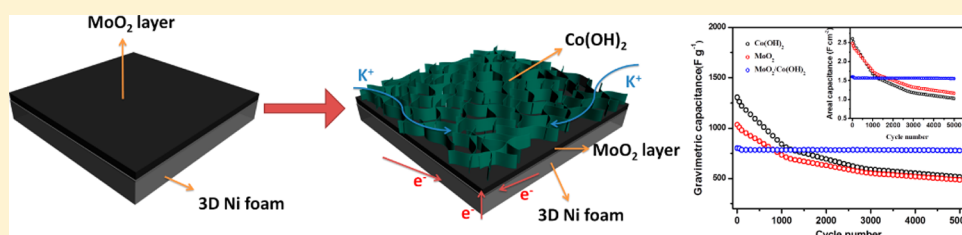
ABSTRACT: Pseudocapacitors have demonstrated an ability to deliver high energy and power densities. The main limitation is their poor cyclability and for this reason the architectural design of electrode materials has attracted considerable attention. Here we report the synthesis of hierarchical nanostructured material by growing Co(OH)$_2$ nanoflakes onto MoO$_2$ thin film. The electrode material exhibits a high capacitance of 800 F g^{-1} at 20 A g^{-1} with only 3% capacitance loss after 5000 cycles and high rate capability with increasing current density from 2 to 40 A g^{-1}, which are better than those of individual component. The enhanced pseudocapacitor performances benefit from the synergistic effect of the hierarchical nanostructure: (1) faster ion diffusion and electron transport at electrode/electrolyte interface, and (2) mitigation of the electrode destruction caused by ion insertion/deinsertion during charge-storage process. This facile design and rational synthesis offers an effective strategy to enhance the electrochemical performance of pseudocapacitors and shows promising potential for large-scale application in energy storage.

KEYWORDS: Synergistic effect, hierarchical material, electrodeposition, molybdenum dioxide, pseudocapacitance, energy storage

Pseudocapacitors (PCs) have attracted considerable attention in the field of energy storage owing to their high capacitance, fast charge–discharge rate, and high power density, which fill the gap between the conventional batteries and capacitors in term of electrochemical performances.[1−4] In pseudocapacitors, more analogously to battery, energy is stored through a reversible adsorption of small-size ions (Li$^+$, Na$^+$, K$^+$, etc.) and faradaic reactions taking place on the surface as well as in the bulk materials. These two contributions lead to high capacitance and high energy density over electrochemical double layer capacitors (EDLCs).[5−7] However, compared with EDLCs, they present poor rate capability and cyclability, which their disadvantages and prevent them from many important applications such as mobile devices, electric and hybrid electric vehicles, and so forth.[8] Thus, the design and rational synthesis of electrode materials with high energy density, high rate capability, and cyclability for pseudocapacitors are a great challenge.

Numerous studies have demonstrated that the charge–storage properties of pseudocapacitors depend not only on the nature of electrode materials but also greatly on the design of these electrodes. To improve the ion diffusion kinetics and electron transport at the electrode/electrolyte interface, the strategy tends to combine different electrode materials in various architecture designs.[9−11] Recently, many researches have been conducted on carboneous materials,[12−17] transition-metal oxides and hydroxides,[17,18] conducting polymers,[19,20] and hybrid composites[10,20−26] as electrode for supercapacitors. However, much attention has been paid on choosing suitable pseudocapacitive materials and their assemblies in appropriate architecture (core/shell, hybrid structure, and so forth) to achieve better performance. Thus, pseudocapacitive metal oxides such as MnO$_2$, RuO$_2$, Co$_3$O$_4$, MoO$_2$, NiO$_2$, and so forth are combined with metal hydroxides, carboneous materials, and conducting polymers in various designs to form hybrid nanostructured electrodes.[16,23,25−28] Among these metal oxides, MoO$_2$ is a suitable candidate for this approach owing to its low cost, low toxicity, low metallic resistivity (8.8 × 10^{-5} Ω·cm), natural abundance, and different oxidation state of molybdenum.[29−32] Furthermore, metal hydroxides, especially Co(OH)$_2$, are good pseudocapacitive candidates and have attracted much interest in recent years due to their layered structure with large interlayer spacing, good reversibility, low
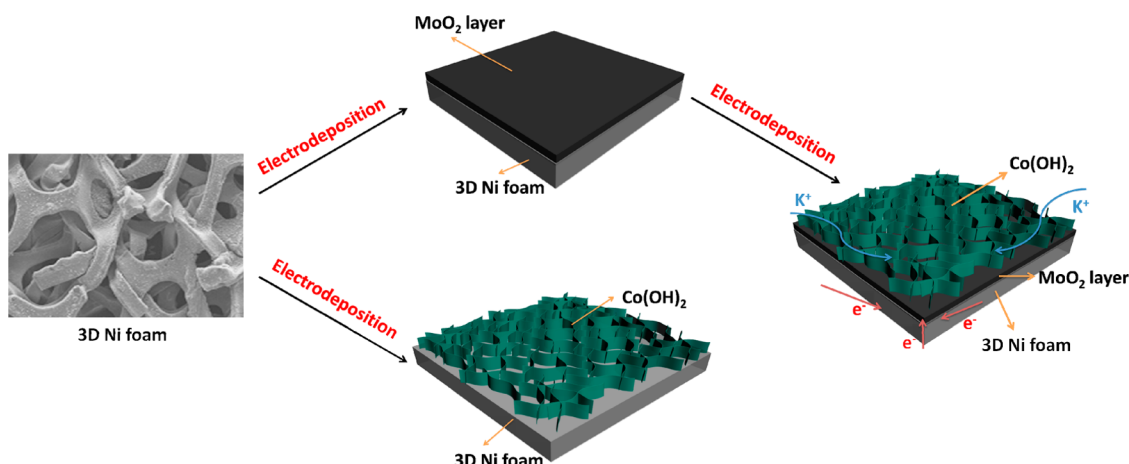
Figure 1. Schematic illustration of the synthesis procedure of hierarchical nanostructured $MoO_2/Co(OH)_2$.
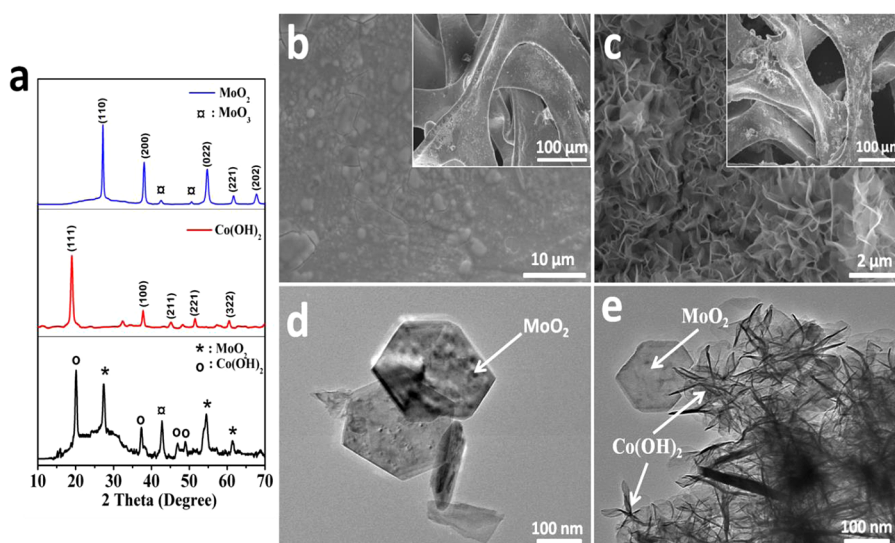
Figure 2. Materials characterization. (a) XRD patterns of MoO_2, $Co(OH)_2$, and hierarchical nanostructured $MoO_2/Co(OH)_2$, respectively. FE-SEM and TEM images of MoO_2 thin film onto three-dimensional Ni foam scaffold (b,d) and MoO_2 thin film coated by $Co(OH)_2$ nanoflakes (c,e), respectively.

cost, easy preparation, high capacitance and well-defined electrochemical redox activity.[33] However the main weakness of both these pseudocapacitive materials is poor rate capability and cyclability.

To realize high-performance supercapacitor for large-scale applications, we design and rationally synthesize hierarchical nanostructured MoO_2 thin film coated by $Co(OH)_2$ nanoflakes onto three-dimensional nickel foam scaffold. The MoO_2 thin film serves as conductive layer for electron transport while $Co(OH)_2$ nanoflakes allow fast ion diffusion owing to their large interlayer space. In our approach, we focus not only on designing hierarchical nanostructured electrode material but also on the synergistic effect of the combination of MoO_2 thin film (good electric conductivity) and $Co(OH)_2$ nanoflakes (large interlayer space). Hence, this design of binder-free electrode enhances the ion diffusion as well as electron transport at the electrode/electrolyte interface. As a result, the hierarchical nanostructured $MoO_2/Co(OH)_2$ exhibits excellent rate capability and long lifespan compared with individual compound.

Here, the design and facile synthesis of hierarchical nanostructured $MoO_2/Co(OH)_2$ by successive electrodeposi-

tion is schematically illustrated (Figure 1). First, MoO_2 thin film was electrodeposited onto clean three-dimensional nickel foam scaffold. Second, the as-deposited MoO_2 thin film serves as substrate for subsequent growth of $Co(OH)_2$ nanoflakes.[34] The samples with different mass ratio of MoO_2 and $Co(OH)_2$ are obtained by adjusting electrodeposition current intensity and time for each single component (Supporting Information, Table S1). On the basis of Pourbaix diagram (Supporting Information, Figure S1),[35] conducting electrochemical deposition in potential range of −0.8 to −0.5 V in the pH between 8 and 10, molybdenum(VI) can be reduced from MoO_4^{2-} ions to Mo (IV) with formation of MoO_2 following the reaction[36]

$$MoO_4^{2-} + 2H_2O + 2e^- \rightarrow MoO_2 + 4OH^- \qquad (1)$$
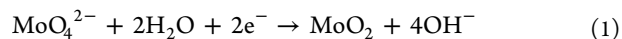
On the other hand, the synthesis of $Co(OH)_2$ could be carried out using electrodeposition in a potential range from −0.9 to −0.2 V and the reaction mechanism is proposed below[25]

$$NO_3^- + H_2O + 2e^- \rightarrow NO_2^- + 2OH^- \qquad (2)$$

$$Co^{2+} + 2OH^- \rightarrow Co(OH)_2 \qquad (3)$$
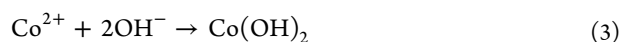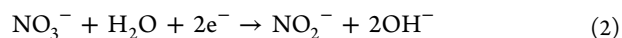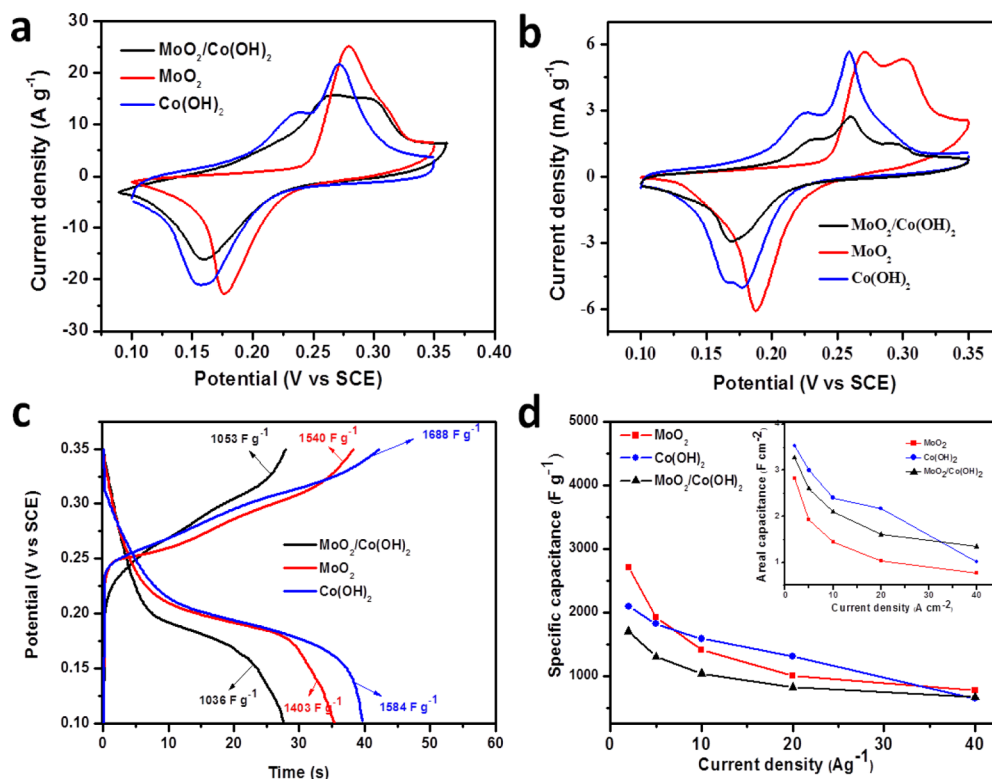
Figure 3. CV curves of MoO_2 thin film, $Co(OH)_2$ nanoflakes and $MoO_2/Co(OH)_2$ at 5 mV s^{-1} (a) and at 1 mV s^{-1} (b), galvanostatic charge/discharge at 10 A g^{-1} (c), and gravimetric (areal inset figure) capacitance versus current increase (d).

X-ray diffraction (XRD) patterns of samples (Figure 2a) were collected with a D8 Advance X-ray diffractometer, using Cu Kα radiation (λ = 1.5418 Å). The main peaks position of the electrodeposited MoO_2 thin film are consistent with monoclinic MoO_2 (JCPDS card No. 33-0929) with a $P21/c$ space group and lattice parameters of a = 5.5900 Å, b = 4.8200 Å, and c = 5.5100 Å. A small amount of impurity corresponding to MoO_3 is observed, which is probably due to the oxidation of MoO_2 during the synthesis process. The XRD patterns for $Co(OH)_2$ nanoflakes are consistent with hexagonal β-$Co(OH)_2$ (JCPDS card No. 74-1057).[37] The diffraction peaks of the hierarchical nanostructured material are consistent with both monoclinic MoO_2 and hexagonal β-$Co(OH)_2$. A peak at 42° related to MoO_3 is also observed, which is due to the oxidation of the first synthesized MoO_2 during the followed electrodeposition of $Co(OH)_2$. The XRD pattern of hierarchical nanostructured $MoO_2/Co(OH)_2$ indicates that our product is constituted by MoO_2 and $Co(OH)_2$.

Top-view field emission scanning electronic microscopic (FE-SEM) images of the as-prepared materials reveal the structural morphology of MoO_2, $Co(OH)_2$ and hierarchical nanostructured $MoO_2/Co(OH)_2$ (Figure 2b,c and Supporting Information, Figure S2b,c).[38] Furthermore, transmission electronic microscopic (TEM) images confirm the hierarchical nanostructure morphology of uniformly electrodeposited MoO_2 thin film onto three-dimensional nickel foam well coated by interconnected $Co(OH)_2$ nanoflakes (around 6 nm thickness) (Figure 2d,e). The growth mechanism of $Co(OH)_2$ nanoflakes on MoO_2 film is probably explained by "oriented attachment" and "self-assembly" as demonstrated in our previous work.[39] The $Co(OH)_2$ nanocrystals are electrodeposited and well attached on MoO_2 thin film, then act as active sites for preferential nucleation because of their lower

surface energy, and thus decrease the free energy barrier and facilitate subsequent nucleation. The as-grown mesocrystals self-assemble to form interconnected nanoflakes. This mechanism leads to strong attachment of $Co(OH)_2$ nanoflakes onto MoO_2 film surface with a stable $MoO_2/Co(OH)_2$ interface. With increasing the deposition time, nanoflakes self-assemble into nanoflowers (Supporting Information, Figure S3d).

To explore the electrochemical performance, we carried out cyclic voltammetry (CV) and galvanostatic charge-discharge tests using a standard three-electrode electrochemical cell containing 2 M KOH aqueous electrolyte. Figure 3a depicts CV curves at scan rate of 5 mV s^{-1} and in the potential range of 0.1 to 0.35 V vs Ag/KCl saturated calomel electrode (SCE) where both electrode materials have redox activities. MoO_2 thin film displays a redox couple at 0.284 and 0.176 V while $Co(OH)_2$ nanoflakes have a redox couple at 0.271 and 0.158 V. The hierarchical nanostructured $MoO_2/Co(OH)_2$ displays two small anodic peaks at 0.266 and 0.294 V and one cathodic peak at 0.162 V that are related to the well-defined peaks of individual compound, suggesting that both materials are involved in electrochemical process. To confirm this assumption, the CV test at 1 mV s^{-1} in the same range was conducted (Figure 3b). The curves of MoO_2 thin film and $Co(OH)_2$ nanoflakes present two peaks at 0.273 and 0.30 V and at 0.226 and 0.260 V for the anodic process and one peak at 0.188 and 0.175 V for cathodic process, respectively. Hierarchical nanostructured $MoO_2/Co(OH)_2$ presents three anodic peaks at potential of 0.296, 0.269, and 0.230 V and one cathodic peak at 0.168 V (Figure 3b). Compared with each component taken individually, a shift on the value of anodic and cathodic peaks is observed but the peaks at 0.296 and 0.230 V are related to the peaks at 0.30 V of MoO_2 and 0.226 V of $Co(OH)_2$ while the peak at 0.269 V can be related to both
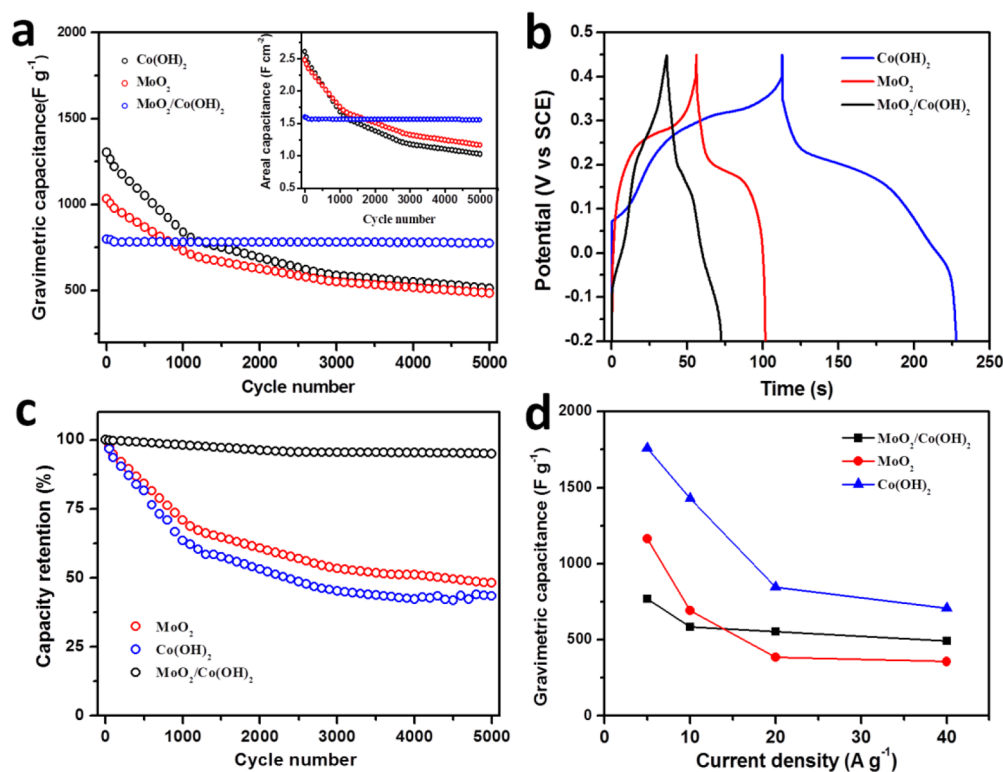
Figure 4. Electrochemical charge−storage performance. (a) Gravimetric and areal (inset figure) cycle performance at 20 A g^{-1}. (b−d) Galvanostatic charge/discharge at 10 A g^{-1} (b), cycling performance at 10 A g^{-1} after 5000 cycles (c), and capacity versus current increase curves (d) of MoO$_2$/Co(OH)$_2$, MoO$_2$ thin film and Co(OH)$_2$ nanoflakes in potential range of −0.2 to 0.45 V.

peaks at 0.273 and 0.260 V of MoO$_2$ thin film and Co(OH)$_2$ nanoflakes, respectively. The appearances of these curves confirm the fact that both materials synergistically contribute to the charge-storage process. The charge transfer mechanism following this electrochemical process can be described by the below plausible reactions

$$MoO_2 + xK^+ + xe^- \leftrightarrow MoO_{2-x}(OK)_x \quad (4)$$

$$MoO_2 + 4OH^- \leftrightarrow MoO_4^{2-} + 2H_2O + 2e^- \quad (5)$$

$$Co(OH)_2 + OH^- \leftrightarrow CoOOH + H_2O + e^- \quad (6)$$

$$CoOOH + OH^- \leftrightarrow CoO_2 + H_2O + e^- \quad (7)$$
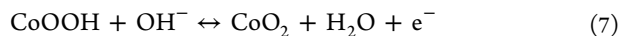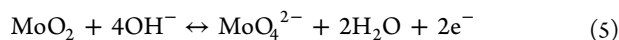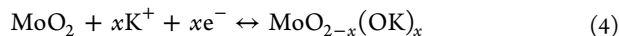
The charge transfer is through adsorption and insertion of potassium ions at the surface and in the electrode material as well as reversible redox reactions,[40,41] as confirmed by the energy dispersive X-ray spectrometric (EDS) mapping analysis taken after cycling (Supporting Information, Figure S3).

The influence of MoO$_2$ loading mass on electrochemical performances was evaluated by synthesizing another two samples (2:1 and 3:1 mass ratio of MoO$_2$ and Co(OH)$_2$ nanoflakes) and performing CV measurements (Supporting Information, Figure S4a,b). With the increase of MoO$_2$ mass in hierarchical nanostructured materials, the CV curves become more rectangular in shape suggesting an electrochemical double layer behavior. The observed redox couple is due to the presence of Co(OH)$_2$ nanoflakes. This behavior demonstrates that when the mass increases (film thickness increases), the MoO$_2$ becomes densely packed with limited accessible surface area and only thin surface layer is involved in the charge

transfer process resulting in "dead volume" and the capacitance decrease (Supporting Information, Figure S4c,d).[42,43]

The areal and gravimetric capacitances are obtained by galvanostatic charge−discharge measurements at different current densities from 2 to 40 A g^{-1}. The capacitance is calculated based on the mass of all active materials loaded on nickel foam scaffold. Figure 3c shows the charge−discharge curves of MoO$_2$ thin film (1.2 mg cm^{-2}), Co(OH)$_2$ nanoflakes (2.0 mg cm^{-2}) and hierarchical nanostructured MoO$_2$/Co(OH)$_2$ (2.5 mg cm^{-2}) at 10 A g^{-1}. The hierarchical nanostructured MoO$_2$/Co(OH)$_2$ exhibits a gravimetric capacitance of 1036 F g^{-1} with 98% Coulombic efficiency while MoO$_2$ thin film and Co(OH)$_2$ nanoflakes present a gravimetric capacitance of 1403 and 1584 F g^{-1} with a Coulombic efficiency of 90 and 93%, respectively. The MoO$_2$ thin film presents defect sites on its surface that act as active sites during the electrochemical process leading to high charge capacitance and low discharge capacitance and thus low Coulombic efficiency. The stable MoO$_2$/Co(OH)$_2$ interface created by growing Co(OH)$_2$ nanoflakes on MoO$_2$ shortens the diffusion pathway for electrolyte ions enhancing the reaction reversibility. Also, the Co(OH)$_2$ nanoflakes considerably reduce the number of defect sites on the surface of MoO$_2$. The two features are responsible for the increased Coulombic efficiency for the hierarchical nanostructured material. Similar phenomena have been reported in lithium ion batteries.[44]

Rate capability, an important factor to evaluate the power application of supercapacitors, is depicted in Figure 3d. Hierarchical nanostructured MoO$_2$/Co(OH)$_2$ displays a gravimetric capacitance decrease from 1697 F g^{-1} at 2 A g^{-1} to 666 F g^{-1} at 40 A g^{-1} with 61% capacitance loss, which is better than those of MoO$_2$ thin film (72%) and Co(OH)$_2$
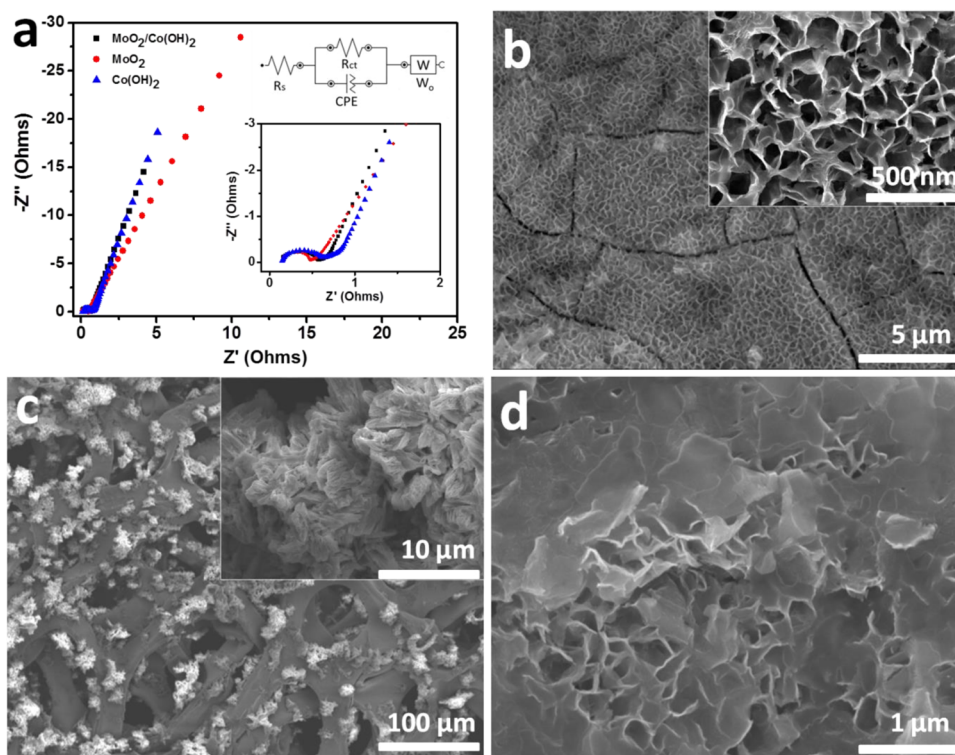
Figure 5. (a) Nyquist plots of $MoO_2/Co(OH)_2$, MoO_2 thin film and $Co(OH)_2$ nanoflakes, FE-SEM images of (b) hierarchical nanostructured $MoO_2/Co(OH)_2$, (c) MoO_2 thin film, and (d) $Co(OH)_2$ nanoflakes after 5000 cycles at 20 A g^{-1}.

nanoflakes (70%). The areal capacitance (inset of Figure 3d) exhibits almost the same behavior. This outstanding electrochemical performance demonstrates that hierarchical nanostructured $MoO_2/Co(OH)_2$ electrode material is more favorable for fast ion diffusion and electron transfer reaction especially at high current density compared with individual component. Another important requirement for supercapacitor applications is cycling stability. Hierarchical nanostructured $MoO_2/Co(OH)_2$ shows 3% capacitance loss after 5000 cycles at 20 A g^{-1} while it is 53 and 61% for MoO_2 thin film and $Co(OH)_2$ nanoflakes, respectively (Figure 4a).

Furthermore, for practical applications of the as-synthesized material, we performed experiments in large potential range between −0.2 to 0.45 V at different current densities (Figure 4b,c). The hierarchical nanostructured $MoO_2/Co(OH)_2$ shows a capacitance of 585 F g^{-1} at 10 A g^{-1} and exhibits only 5% capacitance loss after 5000 cycles, which is better than those reported in the literature,[45−48] while MoO_2 thin film and $Co(OH)_2$ nanoflakes present a gravimetric capacitance of 692 and 1431 F g^{-1} at 10 A g^{-1} with 52 and 57% capacitance loss after 5000 cycles, respectively. The electrochemical impedance spectra (EIS) were used to provide further insights. Nyquist plots taken in frequency range of 0.01 Hz to 10 kHz at open current circuit are shown in Figure 5a. The electrolyte resistances for all electrode materials are around 0.14 Ω. The hierarchical nanostructured electrode has a charge transfer resistance value of 0.58 Ω, which is between those of MoO_2 thin film (0.29 Ω) and $Co(OH)_2$ nanoflakes (0.69 Ω). This value shows the advantage of combining MoO_2 (good electronic conductivity) and $Co(OH)_2$ nanoflakes (large interlayer space) in the hierarchical nanostructured material. FE-SEM images were taken for all the electrode materials after cycling performance (Figure 5b−d). It can be clearly observed

that hierarchical nanostructured $MoO_2/Co(OH)_2$ conserves its morphology while MoO_2 thin film swells and pulverizes, and $Co(OH)_2$ nanoflakes collapse. This demonstrates that the structural destruction caused by ion insertion/deinsertion is mitigated in the novel hierarchical nanostructured $MoO_2/Co(OH)_2$, resulting in the outstanding cyclability compared with the individual compound.

The superior electrochemical performances of hierarchical nanostructured $MoO_2/Co(OH)_2$ electrode materials compared with individual compound is obviously attributed to the following unique features. First, the hierarchical architecture allows synergistic contribution of both materials with increased ion diffusion and fast electron transport. Second, stable $MoO_2/Co(OH)_2$ interface mitigates the destruction of electrode material during charge/discharge cycles (Figure 5b−d).

In summary, we have designed and synthesized hierarchical nanostructured $MoO_2/Co(OH)_2$ by facile and reproducible successive electrodeposition on three-dimensional nickel foam scaffold. This hierarchical architecture allows the synergistic contribution of both materials leading to a better electrochemical performance. The hierarchical nanostructured $MoO_2/Co(OH)_2$ facilitates fast ion diffusion and electron transfer at the electrode/electrolyte interface and also mitigates the structural destruction caused by ion insertion/deinsertion, which results in better capacitance retention versus current density increases. It exhibits a high capacitance of 800 F g^{-1} at 20 A g^{-1} as well as largely enhanced cyclability with only 3% capacitance loss after 5000 cycles than those of MoO_2 (53%) and $Co(OH)_2$ (61%), respectively. Therefore, this facile and rational synthesis strategy offers an effective way to enhance the electrochemical performance of pseudocapacitors and shows a promising large-scale application in energy storage.

Letter

■ ASSOCIATED CONTENT

ⓢ Supporting Information

Additional information and figures. This material is available free of charge via the Internet at http://pubs.acs.org.

■ AUTHOR INFORMATION

Corresponding Author

*E-mail: mlq518@whut.edu.cn.

Author Contributions

[†]K.M.H. and Q.L.W. contributed equally to this work.

Notes

The authors declare no competing financial interest.

■ ACKNOWLEDGMENTS

■ REFERENCES

(1) Simon, P.; Gogotsi, Y. *Nat. Mater.* **2008**, *7*, 845.

(2) Bruce, D.; Kamath, H.; Taracson, J. M. *Science* **2011**, *334*, 928.

(3) Choi, N. S.; Chen, Z.; Freunberger, S. A.; Ji, X.; Sun, Y. K.; Amine, K.; Yushin, G.; Nazar, L. F.; Cho, J.; Bruce, P. G. *Angew. Chem., Int. Ed.* **2012**, *51*, 2.

(4) Miller, J. R.; Simon, P. *Science* **2008**, *321*, 651.

(5) Simon, P.; Gogotsi, Y. *Philos. Trans. R. Soc. London, Ser. A* **2010**, *368*, 3457.

(6) Sharma, P.; Bhatti, T. S. *Energy Convers. Manage.* **2010**, *51*, 2901.

(7) Mai, L.; Li, H.; Xu, L.; Xu, X.; Zhao, Y.; Luo, Y.; Zhang, Z.; Ke, W.; Niu, C.; Zhang, Q. *Sci. Rep.* **2013**, *3*, 1718.

(8) Arico, A. S.; Bruce, P.; Scrosati, B.; Taracson, J. M.; Schalkwijk, W. V. *Nat. Mater.* **2005**, *4*, 366.

(9) Jiang, X. C.; Tian, B. Z.; Xiang, J.; Qian, F.; Zheng, G. F.; Wang, H. T.; Mai, L. Q.; Lieber, C. M. *Proc. Natl. Acad. Sci. U.S.A.* **2011**, *108*, 12212.

(10) Conway, B. E.; Briss, V.; Wojtowicz, J. *J. Power Sources* **1997**, *66*, 1.

(11) Kim, S. K.; Day, R. W.; Cahoon, J. F.; Kempa, T. J.; Song, K. D.; Park, H. G.; Lieber, C. M. *Nano Lett.* **2012**, *12*, 4971.

(12) Ren, Y.; Ma, Z.; Bruce, P. *Chem. Soc. Rev.* **2012**, *41*, 4909.

(13) Qu, D. Y.; Shi, H. *J. Power Sources* **1998**, *74*, 99.

(14) Gamby, J.; Taberna, P. L.; Simon, P.; Fauvarque, J. F.; Chesneau, M. *J. Power Sources* **2001**, *101*, 109.

(15) An, K. H.; Kim, W. S.; Park, Y. S.; Choi, Y. C.; Lee, S. M.; Chung, D. C.; Bae, D. J.; Lim, S. C.; Lee, Y. H. *Adv. Mater.* **2001**, *13*, 497.

(16) Choi, B. G.; Yang, M.; Hong, W. H.; Choi, J.; Huh, W.; Y. S.. *ACS Nano* **2012**, *6*, 4020.

(17) Melet, C.; Rotemberg, B.; Madden, P. A.; Taberna, P. L.; Simon, P.; Gogotsi, Y.; Salanne, M. *Nat. Mater.* **2012**, *11*, 306.

(18) Zhang, Y.; Li, G. Y.; Lu, Y.; Wang, L. Z.; Zhang, A. Q.; Song, Y. H.; Huang, B. L. *Int. J. Hydrogen Energy* **2011**, *B6*, 11760.

(19) Zhou, W. J.; Xu, M. W.; Zhao, D. D.; Xu, C. L.; Li, H. L. *Microporous Mesoporous Mater.* **2009**, *117*, 55.

(20) Snook, A. G.; Kao, P.; Best, A. S. *J. Power Sources* **2011**, *196*, 1.

(21) Wang, K.; Huang, J. Y.; Wei, Z. X. *J. Phys. Chem. C* **2012**, *114*, 8062.

(22) Bordjiba, T.; Belanger, D. *J. Electrochem. Soc.* **2009**, *156* (5), A378.

(23) Bao, L. H.; Zhang, J. F.; Li, X. D. *Nano Lett.* **2011**, *11*, 1215.

(24) Yu, G.; Hu, L.; Liu, N.; Wang, H.; Vosgueritchian, M.; Yang, Y.; Cui, Y.; Bao, Z. *Nano Lett.* **2011**, *11*, 4438.

(25) Xia, X. H.; Tu, J. P.; Zhang, Y. Q.; Mai, Y. J.; Wang, X. L.; Gu, C. D.; Zhao, X. B. *J. Phys. Chem. C* **2011**, *115*, 22662.

(26) Liang, H.; Dongchang, C.; Yong, D.; Shi, F.; Zhong, L. W.; Meilin, L. *Nano Lett.* **2013**, *13*, 3135.

(27) Xia, X. H.; Tu, J. P.; Zhang, Y. Q.; Wang, X. L.; Gu, C. D.; Zhao, X. B.; Fan, H. J. *ACS Nano* **2012**, *6*, 5531.

(28) Liu, J.; Jiang, J.; Cheng, C.; Li, H.; Zhang, J.; Cong, H.; Fan, H. J. *Adv. Mater.* **2011**, *23*, 2076.

(29) Farsi, H.; Gobal, F.; Raissi, H.; Moghiminia, S. *J. Solid State Electrochem.* **2010**, *14*, 643.

(30) Patil, R. S.; Uplane, M. D.; Patil, P. S. *Appl. Surf. Sci.* **2006**, *252*, 8050.

(31) Sinkeviciure, D.; Baltrusaitis, J.; Dukstein, N. *J. Solid State Electrochem.* **2011**, *15*, 711.

(32) Effelson, C. A.; Flores, O. M.; Ha, S.; Norton, M. G. *J. Mater. Sci.* **2012**, *47*, 2057.

(33) Xue, T.; Wang, X.; Lee, J. M. *J. Power Sources* **2012**, *201*, 382.

(34) Preparation of hierarchical nanostructured $MoO_2/Co(OH)_2$: Three dimensional nickel foam 1×1 cm^2 in size was cleaned with diluted nitric acid and then with ethanol and double-distilled water prior to being used as the working electrode. Electrodeposition was conducted in standard three-electrode electrochemical cell with Pt foil, saturated Ag/KCl electrode and the nickel foam as the counter, reference, and working electrode, respectively. The electrodeposition bath was an aqueous solution containing 0.1 M $(NH_4)_6Mo_7O_{24}\cdot4H_2O$ and 1 M NH_4Cl, and some droplets of NH_3 were added to adjust the pH value between 8 and 10. The experiment was performed in potential range of −0.4 to −0.8 V at constant current of 10 mA cm^{-2} at 25 °C for different deposition times. The obtained electrode was washed several times in ethanol and then used for the further synthesis. The $Co(OH)_2$ nanoflakes was obtained by electrodeposition with the previously synthesized MoO_2 thin film onto nickel foam as working electrode in aqueous electrolyte consisting of 1.0 M $Co(NO_3)_2$ and 0.1 M $NaNO_3$ in potential range of −0.2 to −0.9 V at a constant current of 10 mA cm^{-2}. The weight of MoO_2 and $Co(OH)_2$ were determined by calculating the weight difference between the three-dimensional nickel foam, MoO_2 thin film, and $Co(OH)_2$ nanoflakes before and after electrodeposition.

(35) Pourbaix, M. *Atlas of electrochemical equilibria in aqueous solutions*, 2nd ed.; National Association of Corrosion: Houston, TX, 1974.

(36) Zach, M. P.; Inazu, K.; Ng, K. H.; Hemmiger, J. C.; Penner, R. M. *Chem. Mater.* **2002**, *14*, 3206.

(37) Choi, B. G.; Yang, M.; Jung, S. C.; Lee, K. G.; Kim, J.; Park, H.; Park, T. J.; Lee, S. B.; Han, Y.; Huh, Y. S. *ACS Nano* **2013**, *7*, 2453.

(38) The microstructures were observed by field-emission scanning electron microscopy (FE-SEM) (JEOL-7100F), and the transmission electron microscopy (TEM) (JEM-2100F).

(39) Mai, L. Q.; Yang, F.; Zhao, Y. L.; Xu, X.; Xu, L.; Luo, Y. Z. *Nat. Commun.* **2011**, *2*, 381.

(40) Torsten, B.; John, W.; Sarah, H. T.; Bruce, D. *Nat. Mater.* **2010**, *9*, 146.

(41) Wen, S.; Lee, J. W.; Yeo, I. H.; Park, J.; Mho, S. *Electrochim. Acta* **2004**, *50*, 849.

(42) Park, B. O.; Lokhande, C. D.; Park, H. S.; Jung, K. D.; Jo, C. S. *J. Power Sources* **2004**, *134*, 148.

(43) Hou, Y.; Cheng, Y. W.; Hobson, T.; Liu, J. *Nano Lett.* **2010**, *10*, 2727.

(44) Hao, F. B.; Zhang, Z. W.; Yin, L. W. *ACS Appl. Mater. Interface* **2013**, *5*, 8337.

(45) Li, X.; Shao, J.; Li, J.; Zhang, L.; Qu, Q.; Zheng, H. *J. Power Sources* **2013**, *237*, 80.

(46) Zhou, Y.; Lee, C. W.; Kim, S. K.; Yoon, S. *ECS Electrochem. Lett.* **2012**, *1*, A17.

(47) Zheng, L.; Xu, Y.; Jin, D.; Xie, Y. *J. Mater. Chem.* **2010**, *20*, 7135.
(48) Sanchez, B. M.; Brousse, T. C.; Castro, R.; Nicolosi, V.; Grant, P. S. *Electrochim. Acta* **2013**, *91*, 253.